CHARACTERISATION AND EXCURSION MODELLING OF AUDIO HAPTIC TRANSDUCERS

Stephen Oxnard, Ethan Stanhope, Laurence J. Hobden and Mahmoud Masri

Meridian Audio Ltd.
Huntingdon, UK
`stephen.oxnard@meridian.co.uk`

ABSTRACT

Statement and calculation of objective audio haptic transducer performance metrics facilitates optimisation of multi-sensory sound reproduction systems. Measurements of existing haptic transducers are applied to the calculation of a series of performance metrics to demonstrate a means of comparative objective analysis. The frequency response, transient response and moving mass excursion characteristics of each measured transducer are quantified using novel and previously defined metrics. Objective data drawn from a series of practical measurements shows that the proposed metrics and means of excursion modelling applied herein are appropriate for haptic transducer evaluation and protection against over-excursion respectively.

1. INTRODUCTION

Audio haptic transducers, as applied in sound reproduction systems, convey additional tactile sensory input to a listener by means of mechanical vibration of surfaces that are coupled to (in contact with) the listener. This has the effect of enhancing the perception of reproduced sound by inclusion of additional sensory information which would be present for high sound pressure level (SPL) real world sound sources. Evoking vibrotactile sensations that are congruent with the aural reception of airborne sound results in the rendering of a perceptually realistic and immersive multi-sensory experience of high SPL audio. Additionally, haptic systems may be employed to augment the listening experience through enhancement of sonic components (particularly those at low or infrasonic frequencies) to increase a listener's engagement and sense of presence within the reproduced soundfield. Hence, haptic technologies are increasingly employed in sound reproduction systems in gaming, cinema, virtual reality and automotive settings (see e.g. [1, 2, 3, 4]).

The human somatosensory system is the mechanism responsible for rendering perceptible vibrations within the frequency range of 0.3 Hz to 1 kHz [5]. In particular, stimulation of the Pacinian corpuscles (the main mechanoreceptor for vibration) facilitates the perception of vibration with a frequency response ranging up to 500 Hz [6]. Given that the majority of audio content is rendered to match the bandwidth of the human auditory system (20 Hz to 20 kHz) it is reasonable to derive audio haptic signals from the 20 - 500 Hz of full bandwidth audio. As this is the bandwidth of interest, the analysis strategies presented in the following are limited to an upper analysis frequency of 1 kHz to incorporate the

500 Hz octave band and to also align with the upper limit of the somatosensory system.

The main contribution of this work is the verification of characterisation and performance evaluation metrics for haptic transducers as applied in the bandwidth noted above. A novel "Force Potential" metric is introduced as a measurement for moving magnet haptic transducers akin to standardised sensitivity measurements for loudspeaker drive units. Furthermore, it is demonstrated that small signal equivalent lumped-parameter models can be used to predict moving mass excursion, thus providing a means of real time protection against over-excursion in haptic transducers. Previously explored metrics, namely Fall Time and Transient to Late Energy Ratio (TLER) [7], are shown to be relevant to the characterisation of haptic transducers under loaded conditions akin to an installed use case. The definitions of Fall Time and TLER are extended to Rise Time and Transient to Total Energy Ratio (TTER) as a means of characterising systems that exhibit significant pre-ring / pre-echo. All methods of analysis and metrics are also applied to demonstrate the role and impact of resonance reduction audio-tactile signal filtering as an example of simple system tuning strategies.

2. PREVIOUS WORK

The objective evaluation and characterisation of audio haptic transducers has been described alongside investigation of driving signal dynamics processing in related research [7, 8]. This previous work involved measurements of different haptic transducers in approximated simply supported ("free") conditions with no added mass with and without resonance reduction filtering (applied to sharpen transient response profiles). Specifically, [7] provides an initial definition for and example application of Fall Time and TLER as haptic transducer evaluation metrics. Lumped-parameter modelling and numerical simulation of a haptic transducer device was exhibited and discussed in [9] which also provides a novel metric for quantifying harmonic distortion resulting when transducers are driven into largely non-linear modes of operation. Given that haptic systems are becoming increasingly commonplace in immersive audio reproduction systems, it is necessary to continue work on the quantification of the transducers used in these systems drawing on previous procedures and findings.

Building on existing research, this work provides further exposition and demonstration of objective characterisation processes for moving magnet audio haptic transducers. Following a similar procedure as that documented in [9], linear lumped-parameter models are derived for the transducer units measured in this work. These models are then applied to the prediction of magnet excursion which, in turn, can be used to inform over-excursion prevention processes in real-time. As an extension of the work of [7, 8],

measurement, objective characterisation procedures and metrics are refined, expanded and applied to the examination of several moving magnet audio haptic transducers under loaded conditions (as opposed to simply supported, free).

3. HAPTIC DEVICE MEASUREMENTS

3.1. Transducer Measurement Method

For the purpose of supporting the claim that the analysis procedures and measurement metrics documented in the following are transducer agnostic, three moving magnet haptic transducers of different physical properties are put under test. These transducers are commercially available and vary in terms of power handling rating, physical dimensions, magnet weight, chassis materials, suspension build and coil impedance. Table 1 provides a summary of key known quantities for the transducers denoted Drivers 1-3.

Table 1: *Parameters of the 3 transducers under test.*

Parameter	Driver 1	Driver 2	Driver 3
Weight (kg)	78.8	145.6	1,232.0
Surface Area (cm^2)	18.8	8.1	132.7
Power Rating (Wrms)	1	20	75

Each transducer was rigidly affixed to a solid mass of at least 10x the total transducer mass (kg) following the description of full load conditions prescribed in [9]. All measurements were performed in an anechoic environment with the intended radiating surface of each transducer coupled to a horizontal surface of the loading mass. In this way, due to the design of all transducers tested, the suspension of the moving magnet was horizontal with the moving mass acting in the vertical direction.

3.1.1. Electrical Measurement

Measurements of the voltage across the terminals of each transducer, in the test arrangement, were taken in order to derive linear lumped-parameter models. Specifically, the parameters for an LR2 model were obtained for each transducer using an Audio Precision APx525 and APx1701 Transducer Interface for the purpose of providing source signals and measurement via the APx500 measurement software [10]. Impedance and Theile/Small parameter measurements were taken by means of the added mass technique (see e.g. [11]). The resulting LR2 models were then applied to excursion modelling and prediction described in Sec. 4.4 and 5.3.

3.1.2. Accelerometer Measurement

Measurements of magnet displacement were conducted using a Brüel & Kjæl Type 4375 accelerometer attached to the centre of the moving mass in each of the 3 transducers tested. In turn, the accelerometer was connected to a Brüel & Kjæl Type 2635 charge amplifier to provide the necessary translation of charge to voltage with a known voltage-displacement factor. As with the electrical measurements, an Audio Precision APx525 was used in combination with an Audio Precision APx1701 to simultaneously provide drive signals and record responses.

Displacement Impulse Responses (IRs) were measured using Exponential Sine Sweep (ESS) stimuli [12] with a frequency range of 20 Hz to 2 kHz rendered at a sampling rate of 192 kHz. The
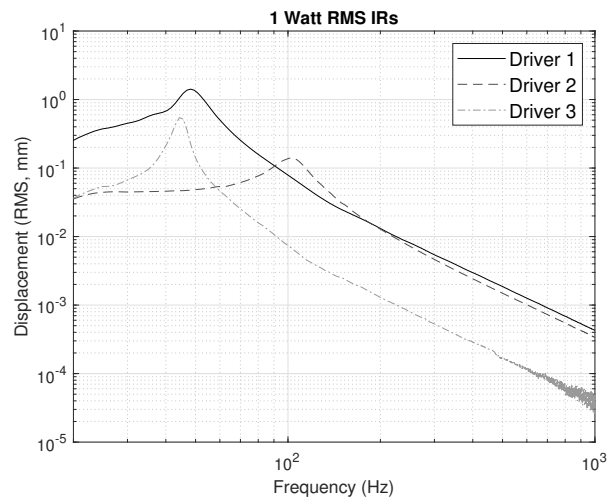

Figure 1: *Frequency domain representation of displacement IRs measured for Drivers 1-3 for 1 Wrms input ESS power.*

ESS signals were 1s in length and were calibrated such that, for each transducer, the power dissipated in the unit would be 1 Wrms and 0.25, 0.50, 0.75 and 1.00 times the rated rms power (W) of each unit. ESS signals with resonance reduction filtering (see Sec. 3.2) were also applied to generate IRs in this way.

A further driving signal was an audio excerpt composed of electronic percussion samples. The same series of power ratings and application of resonance reduction filtering was applied to the percussion signal for the purpose of analysis. The displacement measurements of transducers driven with the percussion driving signal were taken in order to assess the extent to which an LR2 linear excursion model can represent actual moving mass displacement when reproducing programme material.

3.2. Resonance Reduction Filtering

Following the resonance reduction filtering process documented in [7, 8], a negative (dB) gain 2nd order peaking filter was defined for each transducer to reduce the resonances present in the IRs as shown in Figure 1. The required magnitude reduction over frequency was defined to be that which would yield a flatter magnitude response up to the frequency at which each response begins to roll off. Table 2 displays the design parameters that were used to define the resonance reduction filters which were applied to driving source signals using the biquadratic filter structure.

Table 2: *Design parameters for resonance reduction filters.*

Parameter	Driver 1	Driver 2	Driver 3
f_c (Hz)	49	103	44.7
Q	1.8	2.0	3.6
Gain (dB)	-18	-10	-26

In this way, a series of ESS and percussion driving signals were defined with resonance reduction appropriate to each transducer. The purpose of conducting resonance reduction in this work is to demonstrate that adaptions to the haptic systems are reflected in the analysis procedures and objective metrics applied to trans-
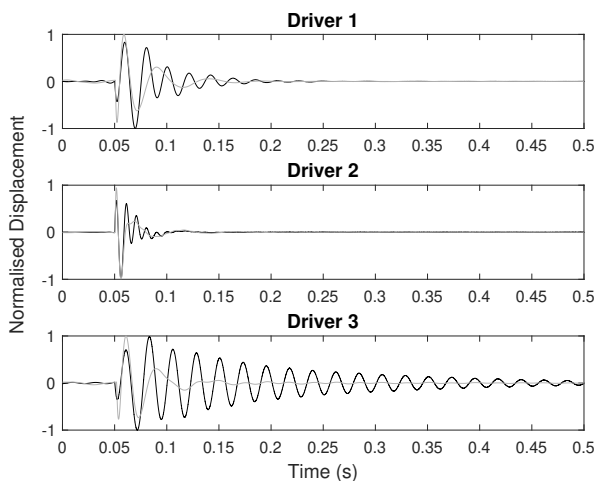
< **338** >

Figure 2: *Displacement IRs pre- and post-resonance reduction filtering (black and grey plots respectively).*

ducer evaluation. The effect of applying resonance reduction filters to the generation of IRs is demonstrated in Figure 2. As shown, it is apparent that the temporal decay profile of all driver IRs is changed under resonance reduction filtering such that decay times are shortened. This is particularly evident in the case of Driver 3. Evaluation of the impact of this filtering strategy on transient response is facilitated by Fall Time and Transient to Late Energy Ratio metrics. These calculated quantities are provided in Sec. 5.2.2.

4. METRICS AND MODELLING

4.1. Force Potential (F_p)

The purpose of Force Potential as an objective measurement of haptic transducers is to provide a quantity equivalent to standardised sensitivity metrics defined to evaluate loudspeaker drive units (see e.g. [13]). The sensitivity of a loudspeaker provides a relationship between driving signal power (W) and output SPL and, therefore, gives insight on how much amplification will be required to reach desired sound levels. In a similar manner, Force Potential is defined simply as the force generated by the moving mass of a haptic transducer noting that, like sensitivity, this quantity is frequency-dependent.

In order to measure Force Potential, an accelerator measurement of the magnet in a moving magnet haptic transducer can be taken by means of the ESS IR capture method [12]. The Force Potential is then defined as the product of acceleration at a given analysis frequency and the moving mass, M_{ms}, of the transducer. In this way, Force Potential is given according to $F_p = ma$ (N). The reason for not denoting this quantity as simply "Force" is drawn from the fact that there is no guarantee that the measured force will be effectively transferred into a coupled surface via chassis fixings or otherwise. Hence, F_p gives a measure of the maximum force that is available to be transferred into a surface material under lossless fixed conditions and serves as a quantity for comparative transducer evaluation as demonstrated in Sec. 5.

4.2. Fall and Rise Times

Fall Time, a metric describing the transient response of a haptic transducer, was introduced in [7] and is calculated from the energy decay curve (EDC) of a measured IR, $h[n]$:

$$EDC[n] = \sum_{k=n}^{\infty} h^2[k] \qquad (1)$$

where $n \in \mathbb{Z}$ is the temporal sample index and ∞ is to be interpreted as the time index at which the IR level reaches the recorded noise floor. The Fall Time is then defined as the time taken for the EDC level to reduce from 90% to 10% of its initial value. As such, this quantity describes the transient capabilities of a given transducer as it measures the time taken for a unit to transition from an excited state to rest.

The definition of Fall Time can be used to inform the definition of an associated metric, Rise Time. Although not applied in this work, Rise Time may find future application in the characterisation of haptic systems which exhibit strong pre-ringing caused, for example, by input driving signal filtering. First, the definition of an Energy Growth Curve (EGC) is given as:

$$EGC[n] = \sum_{k=0}^{n} h^2[k]; n \le pk \qquad (2)$$

where h and n are as previously defined. The temporal sample indices 0 and pk are to be interpreted as the time index where the IR emerges from the recorded noise floor and the IR peak amplitude respectively. The Rise Time is then defined as the time taken for the EGC level to increase from 10% to 90% of its final value, EGC(pk). It is intended that Rise Time be applied to the examination of temporal transient smearing arising from pre-ring. The calculation of Fall/Rise Times facilitates comparison of haptic system transient response characteristics via objective measurements.

4.3. Transient to Late/Total Energy Ratio (TLER and TTER)

The definition of Transient to Late Energy Ratio (TLER) provided in [7] draws inspiration from the standard Early-to-Late Index room acoustics metric [14]. TLER gives a measure of how strong the transient portion of a measured IR is in comparison to the decay portion. Hence, the higher the TLER, the more effective a transducer is in reproducing transient waveforms. In this work, TLER is redefined as a logarithmic quantity (for increased alignment with existing energy ratio metrics such as Clarity, C_{80}, [14]) with an alternative definition of the temporal region of the transient portion, as follows:

$$TLER = 20 \log_{10} \left[\frac{\sum_{k=n_1}^{n_2} h^2[k]}{\sum_{k=n_2}^{\infty} h^2[k]} \right] (\text{dB}) \qquad (3)$$

where: n_1 is the time index of the nearest turning point before the occurrence of the peak absolute IR amplitude value; n_2 is the time index of the nearest turning point after the occurrence of the peak IR amplitude value; ∞ is to be interpreted as the time index at which the IR amplitude descends into the noise floor of the recording. Hence, the transient portion of IRs is defined as the temporal region spanning the first turning points before and after the turning that possesses the maximum absolute amplitude value.

For haptic transducer systems that exhibit pre-ringing as well as transient decay, a new Transient to Total Energy Ratio (TTER)
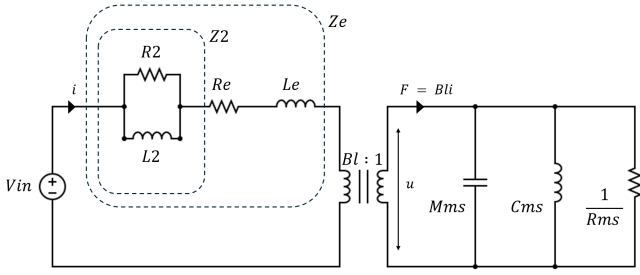
Figure 3: *Electrical and mechanical equivalent circuits comprising the linear lumped-parameter LR2 model used to model magnet excursion for each measured haptic transducer.*

Figure 4: *The network of Figure 3 with simplified electrical circuit containing a single impedance term Z_e.*

Figure 5: *LR2 model with electrical network referred to the mechanical network. This circuit relates magnet velocity $u(\omega)$ and input voltage $V_{in}(\omega)$.*

metric may be applied during comparative performance analysis. TTER is defined as the linear ratio:

$$TTER = \frac{\sum_{k=n_1}^{n_2} h^2[k]}{\sum_{k=0}^{\infty} h^2[k]} \quad (4)$$

where all parameters are as previously defined for TLER and the time index $k = 0$ is to be interpreted as the time at which the signal rises from the noise floor of the IR recording. Given that significant pre-ring was not present in the measured IRs generated for this work, TTER does not find application in this work. Nonetheless, it is intended that TTER be applied in combination with TLER in instances where the transient performance of a transducer is to be quantified when notable pre-ring is present in the response of a given system.

4.4. Excursion Modelling

As previously stated, a linear lumped-parameter LR2 small signal model [15, 16, 17] was chosen to model the behaviour of each transducer. The combination of electrical and mechanical equivalent circuits used in this work is shown in Figure 3. M_{ms} represents the moving mass in the system which, in the case of the transducers measured, is comprised of the mass of the magnet and a portion of the magnet suspension structure. C_{ms} represents the compliance of the magnet suspension and R_{ms} represents losses present in the mechanical system which are mostly associated with the suspension. R_e and L_e are the electrical resistance and inductance of the voice coil respectively. Finally, $R2$ and $L2$ are used to better approximate the electrical behaviour of the transducer at high frequencies where eddy currents become significant. All parameters of the LR2 model of each transducer were calculated via the electrical measurements described in Sec. 3.1.1.

The electrical network, with applied voltage V_{in} and current i, is connected to the mechanical network via an ideal transformer which translates the electrical current i to force flowing through the mechanical network using $F = Bli$ for an electromotive force factor Bl. The velocity of the moving mass, denoted u, is the unit of interest in order to derive moving mass displacement for a given input V_{in}. In order to calculate velocity, the electrical network is referred to the mechanical network. To begin, the equivalent impedance, Z_e (see Figure 4), of all electrical components is given as:
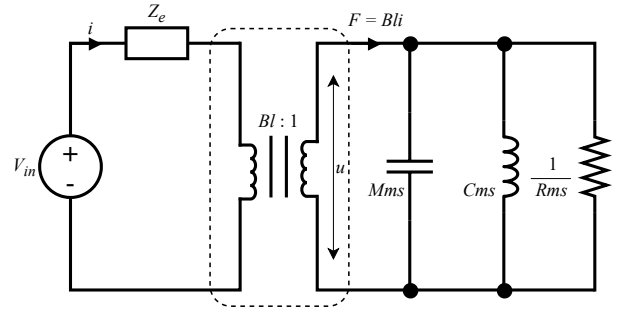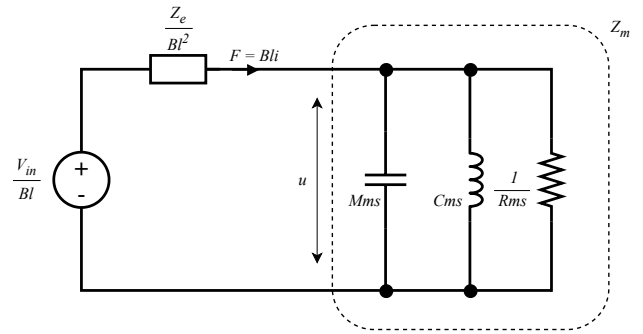
$$Z_e = Z_2 + R_e + L_e \quad (5)$$

where,

$$Z_2 = \frac{R_2 L_2}{R_2 + L_2} \quad (6)$$

To refer the electrical network to the mechanical network, the ideal transformer representing the force factor Bl needs to be removed. Thus, Z_e is divided by the turns ratio of the ideal transformer and V_{in} is divided by the square of the turns ratio. This results in the circuit of Figure 5. The velocity of the moving mass can then be determined as it is the potential across the total mechanical impedance, Z_m:

$$\frac{1}{Z_m} = j\omega M_{ms} + \frac{1}{j\omega C_{ms}} + R_{ms} \quad (7)$$

where ω is radial frequency (rads^{-1}) and j is the imaginary unit. Velocity, $u(\omega)$, may be obtained via a simple potential divider circuit by:

$$u(\omega) = \frac{V_{in}}{Bl} \frac{Z_m}{Z_e + Z_m} \quad (8)$$

from which it is then possible to calculate frequency-dependent displacement for a given V_{in} through integration:

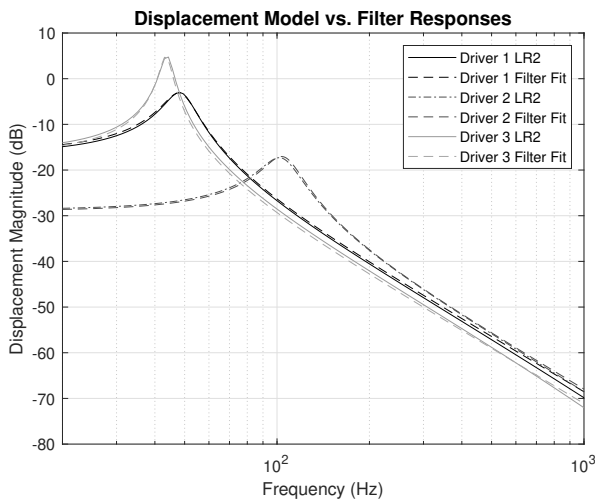$$x(\omega) = \frac{V_{in}}{j\omega Bl} \frac{Z_m}{Z_e + Z_m} \quad (9)$$

< **340** >

Figure 6: *Displacement model (LR2) and derived filter fit responses vs. frequency. NB: DC magnitude offsets shown are arbitrary.*

Figure 7: *Displacement IR frequency response of Driver 1 for ESS stimulus at input rms power levels (W) that are proportions of the unit power rating (1 Wrms).*

As shown in Figure 6, the modelled displacement (via each LR2 model) of the moving mass in the case of each transducer follows a 2nd order low-pass magnitude response. A single 2nd order low-pass biquadratic filter stage was applied to approximate each response. The parameters for each displacement model filter are given in Table 3 and the filter magnitude responses are compared to the LR2 model responses in Figure 6 to demonstrate the goodness of fit.

Table 3: *Design parameters for magnet excursion model (displacement) filters.*

Parameter	Driver 1	Driver 2	Driver 3
f_c (Hz)	48.5	105.2	43.5
Q	4.4	3.9	12

In order to compute the displacement of the moving magnet of each transducer in response to a driving signal, the input driving signal can be filtered using the modelling filters prescribed and scaled for a given signal power. Results of applying this displacement modelling procedure to the case of each haptic transducer under test are given in Sec. 5.3.

5. RESULTS

The evaluation of each measured haptic transducer by means of the metrics and processes described previously is presented in this section. To summarise, accelerometer measurements of 3 audio haptic transducers were taken with each unit reproducing ESS and percussion audio signals, with and without resonance reduction filtering, at rms power levels of 1 Wrms and 0.25, 0.50, 0.75 and 1.00 proportions of the unit rms power ratings. Signal analysis was conducted within a frequency range of 20 Hz - 1 kHz with high- and low-pass filtering applied to input and/or measured output signals as appropriate. The implementation of resonance reduction filtering provides a basis for comparison of calculated metrics to
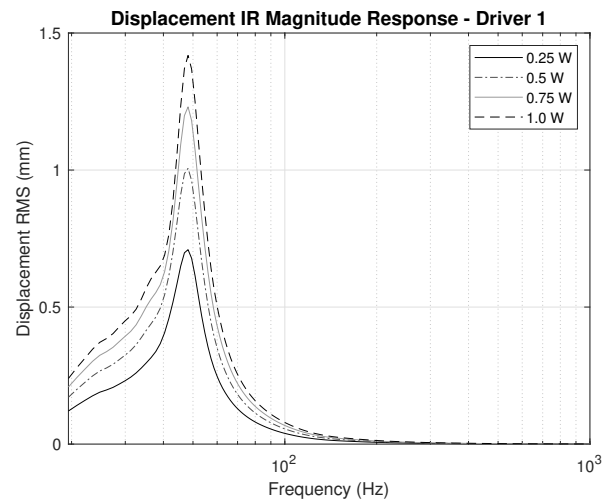
demonstrate the use and application of these metrics for transducer characterisation.

Figure 8: *Displacement IR frequency response of Driver 2 for ESS stimulus at input rms power levels (W) that are proportions of the unit power rating (20 Wrms).*

5.1. IR Frequency Domain Analysis

Displacement measurements taken in response to ESS stimuli at proportions of the rms power rating of each transducer culminated in the rendering of a series of IRs that reveal a relationship between frequency-dependent displacement magnitude and input power in each test case. Figures 7 and 8 display the magnitude displacement vs. frequency at proportional input rms power levels for Drivers 1 and 2 respectively. The purpose of this analysis is twofold. Firstly, it reveals if there is any shift in resonance frequency as the in-
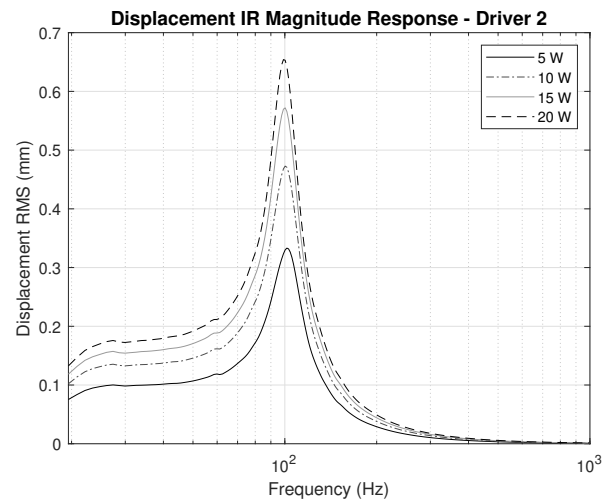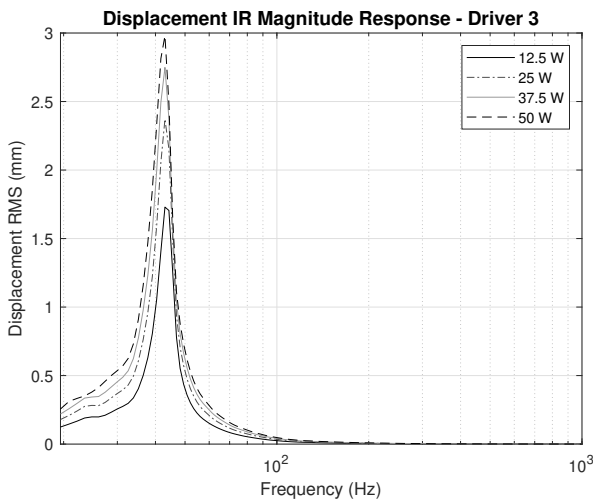
<   **341**   >

Figure 9: *Displacement IR frequency response of Driver 3 for ESS stimulus at input rms power levels (W) that are proportions of the unit power rating (50 Wrms).*

Figure 10: *Force potential vs. frequency for all 3 Drivers measured using 1 Wrms ESS stimulus.*

put power (and hence resulting moving mass displacement) is increased. For Driver 1, no significant shift is evident, while a very small decrease in resonance is observed in the case of Driver 2. Secondly, this analysis shows whether there is an approximate relationship between input power and displacement magnitude. In the case of both Drivers 1 and 2, it may be stated that the displacement magnitude approximately doubles for every quadrupling of input power. This is particularly evident at the resonant frequencies in both cases.

In contrast, the displacement IRs for Driver 3 (as shown in Figure 9) exhibit a significant decreasing shift in resonance frequency with increasing input power. Moreover, the 2x displacement magnitude for 4x input power increase is no longer evident (comparing 12.5 Wrms to 50 Wrms input power). These findings are indicative of nonlinear behaviour, present in the transducer and/or the measurement arrangement, which is exacerbated by increasing input power level. The exact nature of the mechanisms that give rise to such nonlinearities has not been investigated as part of this work and warrants further investigation. Nonetheless, it is apparent that this unit is not capable of operating linearly within its rms power rating and that the twofold displacement increase for fourfold input power increase only holds for input powers up to half the rated power handling. These findings are presented here to better inform the appraisal of metrics as given in the following sections.

5.2. Transducer Characteristics

5.2.1. Force Potential

The F_p measures were calculated using the M_{ms} value taken from the LR2 model derived from electrical measurements for each transducer. In each case, F_p was calculated through multiplication of M_{ms} with acceleration responses taken as the second time derivative of measured displacement IRs.

The resulting frequency-dependent F_p curves are displayed in Figure 10. As shown, each transducer reaches a force maximum at resonance with Driver 3 exhibiting the largest resonant peak compared to both that of Drivers 1 and 2 and the nominal F_p level in the
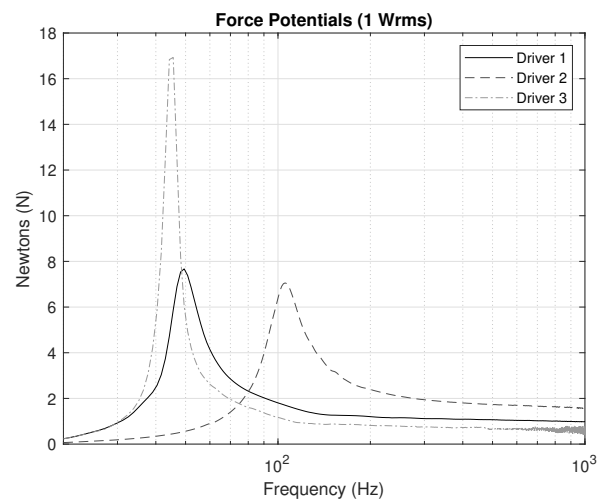
analysis bandwidth. These characteristics are largely in line with expectations given the derived moving masses and the 1 Wrms displacement IRs of Figure 1. The quantification of F_p becomes useful when considering potential applications of the transducers under test. For instance, it is clear from Figure 10 that the smallest unit with the lowest power rating (Driver 1) is capable of producing a larger force than that of the largest and highest rated unit (Driver 3) across the majority of the analysis bandwidth ($f > 50$ Hz). Additionally, it is also shown that Driver 2 possesses the highest F_p above 80 Hz but produces very little output towards low frequencies (20 Hz - 40 Hz) compared to both Drivers 1 and 2.

Findings such as these, in combination with known power ratings, are of value when designing an audio haptic reproduction system where pass band and amplification specifications and/or limitations are prescribed. As an example, evaluation of F_p across the 3 transducers in the test arrangement provides a means of supporting the claim that Driver 1 is the correct choice for a low power consumption system when extension to low frequencies ($f \approx 50$ Hz) is required. Alternatively, if low frequency reproduction is required, Driver 1 and 3 have been shown to provide output down to low frequencies. However, Driver 1 is providing this while operating at its maximum rated level. If further output force is needed, more amplification would be necessary and Driver 3 would have to be selected to avoid damage that could be imposed through overpowering Driver 1. A final point on the use of F_p is that if a given transducer is shown to follow the previously demonstrated 2x displacement magnitude for 4x input power level, a similar 2x force for 4x input power relationship can be applied up to the power rating of the transducer in question.

5.2.2. Fall Times and TLERs

Both Fall Time (FT) and Transient to Late Energy Ratio (TLER) metrics are derived from displacement IRs rendered via accelerometer measurements as per Sec. 3.1.2. IRs were taken across 3 haptic transducers, with and without resonance reduction filtering for 4 levels of input power that were proportions of the power rating of each unit. This range of measurements corresponds to 8 IRs per

<   **342**   >

transducer and provides a means of assessing FT and TLER as a means of transducer system comparison and evaluation.

The FT and TLER metric values calculated from measured displacement IRs are presented in Tables 4, 5 and 6 for Drivers 1 - 3 respectively.

Table 4: *Fall Times (FT) and Transient to Late Energy Ratios (TLER) for Driver 1. Measurements with resonance reduction filtering applied are denoted with subscript RR.*

Power (Wrms)	FT (ms)	FT$_{RR}$ (ms)	TLER (dB)	TLER$_{RR}$ (dB)
0.25	33.6	33.5	8.10	7.61
0.50	34.1	33.6	7.99	7.58
0.75	35.0	33.7	7.86	7.57
1.00	39.2	33.6	7.77	7.59

Table 5: *Fall Times (FT) and Transient to Late Energy Ratios (TLER) for Driver 2. Measurements with resonance reduction filtering applied are denoted with subscript RR.*

Power (Wrms)	FT (ms)	FT$_{RR}$ (ms)	TLER (dB)	TLER$_{RR}$ (dB)
5	18.0	13.8	8.84	16.33
10	18.5	13.0	8.20	16.53
15	18.8	12.7	7.69	16.60
20	19.0	12.5	7.36	16.68

Table 6: *Fall Times (FT) and Transient to Late Energy Ratios (TLER) for Driver 3. Measurements with resonance reduction filtering applied are denoted with subscript RR.*

Power (Wrms)	FT (ms)	FT$_{RR}$ (ms)	TLER (dB)	TLER$_{RR}$ (dB)
12.5	120.8	30.8	-6.83	6.83
25	111.5	32.0	-6.06	6.54
37.5	106.4	32.8	-5.38	6.28
50	100.7	33.4	-4.71	6.03

In terms of Fall Times, it is clear that without resonance reduction filtering, Driver 2 exhibits the shortest temporal decay profile and Driver 3 the longest. This finding correlates well with the F_p profiles given that both Drivers 1 and 3 extend to lower frequencies and have larger resonance peaks than that of Driver 2 (with Driver 3 having the largest resonance of all). Hence, while Driver 2 may be seen as having the best transient reproduction performance, this is in part due to the fact that it does not reproduce low frequencies effectively in the test arrangement. The comparatively large FTs of Driver 3 are consistent with the low TLER values measured without resonance reduction. Comparing TLERs for Drivers 1 and 2, it is evident that while Driver 2 has a significantly faster FT, the transient energy present in the IRs for each largely overlap for the full range of input power levels. Again, this can be said to agree with the F_p profiles suggesting that while Driver 1 has a longer decay profile, the low frequency extension yields greater energy in the initial portion of the IR than that of Driver 2.

The application of resonance reduction filters is reflected well in the measures of FT($_{RR}$) and TLER($_{RR}$). It is noted that, for all 3 Drive units, the filtering process yields more consistent response characteristics across input power levels. This is indicative of each transducer having a more controlled response which is consistent with a reduction in resonant energy. For Drivers 2 and 3, the improvement of transient responses is evidenced by significant reductions in FT and increases in TLER values. The same improvement is not as apparent in the case of Driver 1 where FTs reduce for all input power levels, but TLER values decrease (albeit marginally for both metrics). Referring to Figure 2 (top panel), the transient portions (as defined in Sec. 4.3) of pre- and post-filtered IRs demonstrate that the TLER values are reflecting a slight decrease in transient energy with the application of filtering.

5.3. Excursion Model Evaluation

Accelerometer measurements of each transducer reproducing a sequence of electronic percussion samples were taken at increasing input power levels (proportions of each unit's power rating). Measurements were conducted with and without resonance reduction filtering. The amplitude envelope of resulting recorded displacement signals was derived in order to ascertain excursion magnitude profiles. Using the excursion modelling procedure, the displacement for each transducer and input power level was simulated. The amplitude envelope of each simulated signal was derived to provide predicted excursion magnitude profiles for comparison with the measured data.

In order to evaluate the modelled excursion profiles, the rms error between measured and predicted profiles was calculated for each measurement case. A percentage error quantity was then defined as the ratio (%) of the rms error to the rms signal level of the measured excursion profile. In this way, the error between measurement and prediction is quantified relative to an average metric of the measured excursion profile signal level. Table 7 provides the prediction error calculated for Drivers 1-3. Table 8 provides the error generated for input signals with resonance reduction filtering applied.

Table 7: *Percentage error between measured and predicted excursion for reproduction of electronic percussion audio sample at proportional input power levels.*

Power Proportion	Driver 1 error (%)	Driver 2 error (%)	Driver 3 error (%)
0.25	4.00	6.26	27.52
0.50	3.44	5.64	26.84
0.75	3.19	5.36	26.72
1.00	2.99	5.17	26.87

Table 8: *Percentage error between measured and predicted excursion for reproduction of electronic percussion audio sample at proportional input power levels. Resonance reduction filtering applied.*

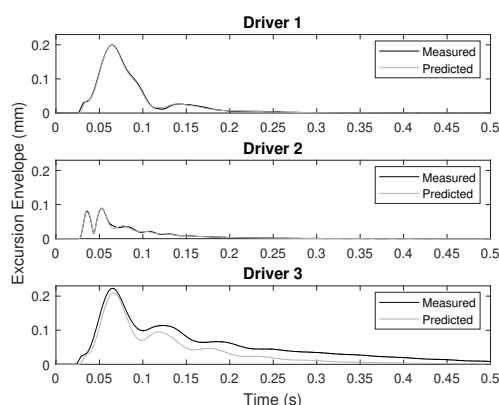| Power Proportion	Driver 1$_{RR}$ error (%)	Driver 2$_{RR}$ error (%)	Driver 3$_{RR}$ error (%)
0.25	3.45	4.74	20.69
0.50	2.90	3.60	19.99
0.75	2.78	3.12	19.54
1.00	2.75	2.80	19.31

< **343** >

Figure 11: *Measured vs. predicted excursion envelopes of input transient signal portion (0.25 power proportion, without resonance reduction filtering) derived for Drivers 1-3.*

The percentage error metrics of Tables 7 and 8 support the claim that the excursion models derived for Drivers 1 and 2 provide a good approximation to the temporal excursion profiles that were measured for each input signal case (with and without resonance reduction filtering) with maximum errors of 4.00 and 6.26 % respectively. The model derived for Driver 3 exhibits less accurate performance with a maximum prediction error of 27.52 %. Figure 11 displays the measured and predicted excursion envelope for a large input amplitude transient event for the worst prediction case for all transducers (0.25 power proportion without resonance reduction). As shown, the predicted excursion is a close approximation to measured for Drivers 1 and 2, while the prediction is consistently lower in the case of Driver 3. It is also shown that the excursion amplitude decay profile of Driver 3 is under represented by the prediction model. In turn, this suggests that the linear lumped-parameter model is not capable of representing resonant and nonlinear behaviour present in this system. This and the trend of decreasing error as input power level increases are to be investigated as part of further work.

6. CONCLUSION

This work has extended investigation into procedures and metrics that can be used to characterise audio haptic transducers. The main contributions are the definition of new IR-based evaluation metrics (F_p, Rise Time and TTER), the refinement of previously suggested metrics (Fall Time and TLER) and exposition of a means of moving mass excursion profiling for the purposes of protection against over-excursion. All metrics have been demonstrated as useful for representing and objectively quantifying haptic system performance by means of practical measurements and analysis thereof. It is intended that the processes and metrics documented here provide a basis for, and a means of influencing, practical audio haptic reproduction system design.

7. REFERENCES

[1] Mauricio Orozco, Juan Silva, Abdulmotaleb El Saddik, and Emil Petriu, "The role of haptics in games," *Haptics Rendering and Applications*, Jan. 2012.

[2] Fabien Danieau, Julien Fleureau, Philippe Guillotel, Nicolas Mollet, Marc Christie, and Anatole Lécuyer, "Toward haptic cinematography: Enhancing movie experiences with camera-based haptic effects," *IEEE MultiMedia*, vol. 21, no. 2, pp. 11–21, 2014.

[3] Yudai Tanaka, Alan Shen, Andy Kong, and Pedro Lopes, "Full-hand electro-tactile feedback without obstructing palmar side of hand," in *Proceedings of the 2023 CHI Conference on Human Factors in Computing Systems*, New York, NY, USA, 2023, CHI '23, Association for Computing Machinery.

[4] Jukka Linjama and Vesa Välimäki, "Immersive personal sound using a surface nearfield source," in *Audio Engineering Society Convention 153*, October 2022, pp. 1–7.

[5] Byron Remache-Vinueza et al., "Audio-tactile rendering: A review on technology and methods to convey musical information through the sense of touch," *Sensors*, vol. 21, no. 19, Sept. 2021.

[6] David Birnbaum and Marcelo Wanderley, "A systematic approach to musical vibrotactile feedback," *International Computer Music Conference, ICMC 2007*, 04 2011.

[7] Stephen Oxnard, Laurence J. Hobden, Ethan Stanhope, Christian S. E. Cotton, and Fraser L. Todd, "Objective measurement for evaluation of haptic audio signals and transducers," in *Proceedings of the Institute of Acoustics*, November 2023, vol. 45, pp. 1–10.

[8] Stephen Oxnard, Ethan Stanhope, and Laurence J. Hobden, "Tactile signal derivation part 2: Extracting haptic information from traditional audio," in *Audio Engineering Society Convention 154*, May 2023, pp. 1–10.

[9] Ravindra Wijesiriwardana, Sarosh Khwaja, Stuart Mansbridge, and Jackie Green, "Towards vibrotactile transducer characterization," in *Audio Engineering Society Convention 155*, Oct 2023, pp. 1–9.

[10] "Audio Precision, APx500 User Manual v8.0," online: https://www.ap.com/download/apx500-user-manual-4/, accessed: 2024-03-18.

[11] Leo Leroy Beranek and Tim Mellow, *Acoustics: sound fields and transducers*, Academic Press, 2012.

[12] Angelo Farina, "Simultaneous measurement of impulse response and distortion with a swept-sine technique," *Journal of the Audio Engineering Society*, february 2000.

[13] *Sound system equipment Part 22: Electrical and mechanical measurements on transducers,* IEC 60268-22:2020, 2020.

[14] International Organization for Standardization, *ISO 3382-1: Acoustics - Measurement of Room Acoustic Parameters. Part 1 : Performance Rooms*, ISO, 2009.

[15] Harry Ferdinand Olson, *Dynamical analogies*, vol. 2729, Van Nostrand Princeton, 1958.

[16] Mark Dodd, Wolfgang Klippel, and Jack Oclee-Brown, "Voice coil impedance as a function of frequency and displacement," in *Audio Engineering Society Convention 117*. Audio Engineering Society, 2004.

[17] Richard H Small, "Vented-box loudspeaker systems–part 1: Small-signal analysis," *Journal of the Audio Engineering Society*, vol. 21, no. 5, pp. 363–372, 1973.

< **344** >